JACS
JOURNAL OF THE AMERICAN CHEMICAL SOCIETY
Article
pubs.acs.org/JACS

Experimental and Computational Investigation of Au_{25} Clusters and CO_2: A Unique Interaction and Enhanced Electrocatalytic Activity

Douglas R. Kauffman,*[,†,‡] Dominic Alfonso,[†] Christopher Matranga,[†] Huifeng Qian,[§] and Rongchao Jin[§]

[†]National Energy Technology Laboratory (NETL), United States Department of Energy, Pittsburgh, Pennsylvania 15236, United States

[‡]URS, P.O. Box 618, South Park, Pennsylvania 15129, United States

[§]Department of Chemistry, Carnegie Mellon University, Pittsburgh, Pennsylvania 15213, United States

Supporting Information

ABSTRACT: Atomically precise, inherently charged Au_{25} clusters are an exciting prospect for promoting catalytically challenging reactions, and we have studied the interaction between CO_2 and Au_{25}. Experimental results indicate a reversible $Au_{25}-CO_2$ interaction that produced spectroscopic and electrochemical changes similar to those seen with cluster oxidation. Density functional theory (DFT) modeling indicates these changes stem from a CO_2-induced redistribution of charge within the cluster. Identification of this spontaneous coupling led to the application of Au_{25} as a catalyst for the electrochemical reduction of CO_2 in aqueous media. Au_{25} promoted the $CO_2 \rightarrow CO$ reaction within 90 mV of the formal potential (thermodynamic limit), representing an approximate 200−300 mV improvement over larger Au nanoparticles and bulk Au. Peak CO_2 conversion occurred at −1 V (vs RHE) with approximately 100% efficiency and a rate 7−700 times higher than that for larger Au catalysts and 10−100 times higher than those for current state-of-the-art processes.

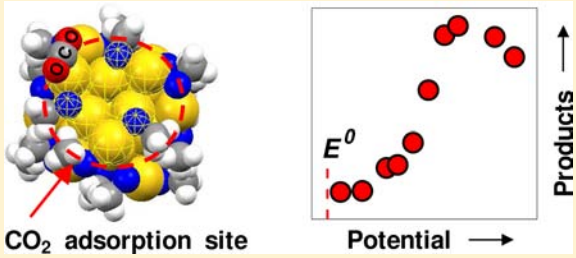

INTRODUCTION

The chemistry of Au surfaces and Au nanoparticles has been the focus of intense study,[1−3] but recent synthetic advances have introduced a new class of "small" ligand-protected Au clusters with unique chemical and electronic properties.[2,4−6] Sub-2-nm clusters differ from larger nanoparticles because their energy levels become quantized and they develop molecule-like electronic structures.[2,4] Crystallographic efforts have confirmed that such small Au clusters form into atomically precise structures and that ligand-protected Au_{25} clusters, possess an inherent anionic (negative) charge.[7,8] Ligand-protected Au_{25} clusters are a unique platform to study catalytic reactions because they bridge the size gap between molecules and larger nanoparticles, they possess an anionic charge, and their surface structure is precisely known. Despite these features, the catalytic activities of Au_{25} and similar atomically precise clusters have only been investigated experimentally for a handful of reactions, such as the oxidation of styrene and cyclohexane,[9−12] the hydrogenation of aldehydes and ketones,[13,14] and the electrochemical reduction of O_2.[15] One particularly appealing catalytic challenge to consider for the negatively charged Au_{25} cluster is the reduction of carbon dioxide. Not only is CO_2 an important greenhouse gas, but it also represents an abundant starting material for the generation of fine chemicals and fuels.[16−19]

Herein we report a spontaneous and reversible electronic interaction between CO_2 and ligand-protected $Au_{25}(SC_2H_4Ph)_{18}^-$ clusters (abbreviated as Au_{25}). *In situ* nonaqueous spectroelectrochemistry was used to manipulate the charge state of Au_{25} and establish a benchmark for adsorbate-induced spectroscopic changes. These benchmarking studies were required to gain insight into the subtle electronic structure changes noted during the coupling of Au_{25} and CO_2 in dimethylformamide (DMF). Specifically, the introduction of CO_2 reversibly induced spectroscopic and electrochemical changes that were similar to those seen during Au_{25} oxidation. We also used density functional theory (DFT) to model the interaction between Au_{25} and CO_2. This type of study is a valuable complement to experimental efforts because it allows direct, atomic-scale determination of favorable binding sites and adsorption structures. Previous computational efforts have considered the binding of adsorbates such as O_2 and CO on ligand-free or partially ligand-protected clusters.[20,21] In our calculations, several physisorbed linear CO_2 states were identified on fully $S-CH_3$ protected Au_{25} clusters. From a theoretical standpoint, first-principles investigations focusing on the adsorption properties of fully ligand-protected clusters are scarce, and relatively little is known about the effects of molecular physisorption on the cluster's electronic structure. Our results correlate experimental and computational data to demonstrate that molecular physisorption can *reversibly* perturb the Au_{25} electronic structure and impact optical and electrochemical properties.

Received: April 4, 2012
Published: May 22, 2012

   dx.doi.org/10.1021/ja303259q | J. Am. Chem. Soc. 2012, 134, 10237−10243

The observation of spontaneous coupling between the negatively charged Au_{25} cluster and CO_2 motivated us to investigate Au_{25} as a catalyst for the electrochemical reduction of CO_2. Typical electrocatalysts require large overpotentials to convert CO_2 into useful products,[16−19] ultimately creating a challenge for large-scale deployment. In this application, Au_{25} catalyzed the two-electron conversion of CO_2 into CO within 90 mV of the formal potential (thermodynamic limit) of −0.103 V vs the reversible hydrogen electrode (RHE).[19] The low overpotential is significant because it represents an approximate 200−300 mV reduction in potential compared to the larger Au nanoparticles and bulk Au tested in this study and those in previously published reports.[18,19,22] Moreover, Au_{25} showed peak $CO_2 \rightarrow CO$ conversion at −1.0 V with approximately 100% Faradaic efficiency and a rate 7−700 times higher than those for the larger Au catalysts tested in this study and 10−100 times higher than those for current state-of-the-art processes.[23] In practical terms, CO is a very useful chemical that can be converted into a variety of valuable hydrocarbon species, and a low-voltage, high-efficiency process for converting CO_2 into CO could be instrumental in developing new carbon management technologies.[16,17]

RESULTS AND DISCUSSION

Spectroelectrochemical Properties of Au_{25}. Figure 1 presents the structure, energy level diagram, and optical spectra of Au_{25}. The structure of Au_{25} contains a Au_{13} core surrounded by a shell of six Au_2S_3 semiring structures (the organic C_2H_4Ph ligands and tetraoctylammonium counterion are shown in Figure S1 of the Supporting Information).[7,8] The origins of the Au_{25} optical absorption spectrum have been interpreted,[8] albeit some uncertainty remains because electronic and geometric coupling between core and shell atoms contribute to the spectral features.[4,24,25] The onset of the absorption spectrum at approximately 1.4 eV corresponds to the energy gap (E_g) between the highest occupied and lowest unoccupied molecular orbitals (HOMO and LUMO).[8,26,27] Recent computational and experimental studies have identified the *a′* and *a* absorbance features as HOMO → LUMO transitions originating from closely spaced, nondegenerate orbitals.[24,25,28] Absorbance feature *b* is attributed to both HOMO → LUMO + $^1/_2$ and HOMO − 2 → LUMO transitions, and absorbance feature *c* represents a HOMO − 5 → LUMO transition. The Au_{25} photoluminescence (PL) profile remained unchanged if excited at absorbance feature *b* (2.78 eV) or *a* (1.81 eV), although excitation at absorbance feature *a* produced lower PL intensity (Figure S2). Equivalent emission profiles at different excitation energies indicate LUMO → HOMO emission,[27] and the PL shoulder at 1.38 eV corresponded to the expected E_g in a variety of solvents. PL below 1.38 eV suggests relaxed emission from midgap states,[27] and the apparent spectral structure below 1.1 eV results from the optical transmittance of the solvent (Figure S3).

The Au_{25} optical absorbance and PL spectra are very sensitive to charge transfer, and characteristic spectral changes have been observed after chemical oxidation with oxygen[29,30] or dissolved cations,[31,32] ligand exchange,[30,33−35] and the application of electrochemical potentials.[27] Accordingly, electrochemical modification of the Au_{25} optical properties provides an excellent benchmark to compare adsorbate-induced changes. Nonaqueous electrochemistry was used to apply oxidizing or reduction potentials to Au_{25} clusters in DMF (Figure S4),[27,36] and the *in situ* spectroelectrochemical oxidation of Au_{25} is presented in Figure 1c. The application of an oxidizing potential bleached the *a′*, *a*, and *b* absorbance features due to electronic depletion of the HOMO.[27] Furthermore, an oxidation-induced geometric change increased both the absorbance at 2.04 eV and the peak area of absorbance feature *c*.[29] The origins of the oxidation-induced PL increase are still debated in the literature,[27,30,33] but the blue-shifted PL maximum suggests that oxidation may inhibit photoexcited electrons from relaxing into midgap states. Both the absorbance and PL changes were qualitatively reversible with the application of a sufficiently reducing potential, but the PL blue shift did not reverse regardless of the applied potential (Figure S5).

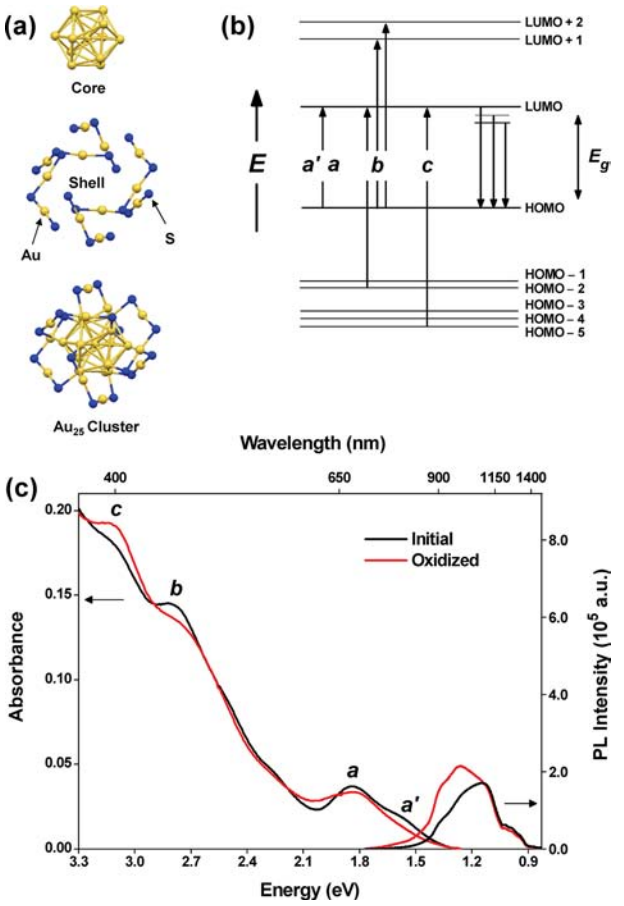

Figure 1. Structure, energy level diagram and spectroelectrochemical properties of Au_{25}. (a) Au_{25} structure: the C_2H_2Ph ligands and tetraoctylammonium (TOA^+) counterion are shown in Figure S1 in the Supporting Information.[7,8] (b) Au_{25} energy level diagram. (c) *In situ* spectroelectrochemistry demonstrating oxidation-induced changes to Au_{25} optical properties in N_2 purged DMF + 0.1 M TBAP; the labeled absorbance features correspond to the transitions identified in panel b.

Interaction between Au_{25} and CO_2. Figure 2a and b presents the optical spectra of an initially N_2 purged Au_{25} solution that was subsequently saturated with CO_2. The introduction of CO_2 bleached the *a′*, *a*, and *b* absorbance features and increased the absorbance at both 2.04 eV and feature *c*. Additionally, the normalized PL maximum showed an increase and blue shift; non-normalized PL spectra are shown in Figure S6 for reference. The spectroscopic changes were reproducible from sample to sample (Table S1) and consistent with those noted during spectroelectrochemical oxidation

dx.doi.org/10.1021/ja303259q | J. Am. Chem. Soc. 2012, 134, 10237−10243

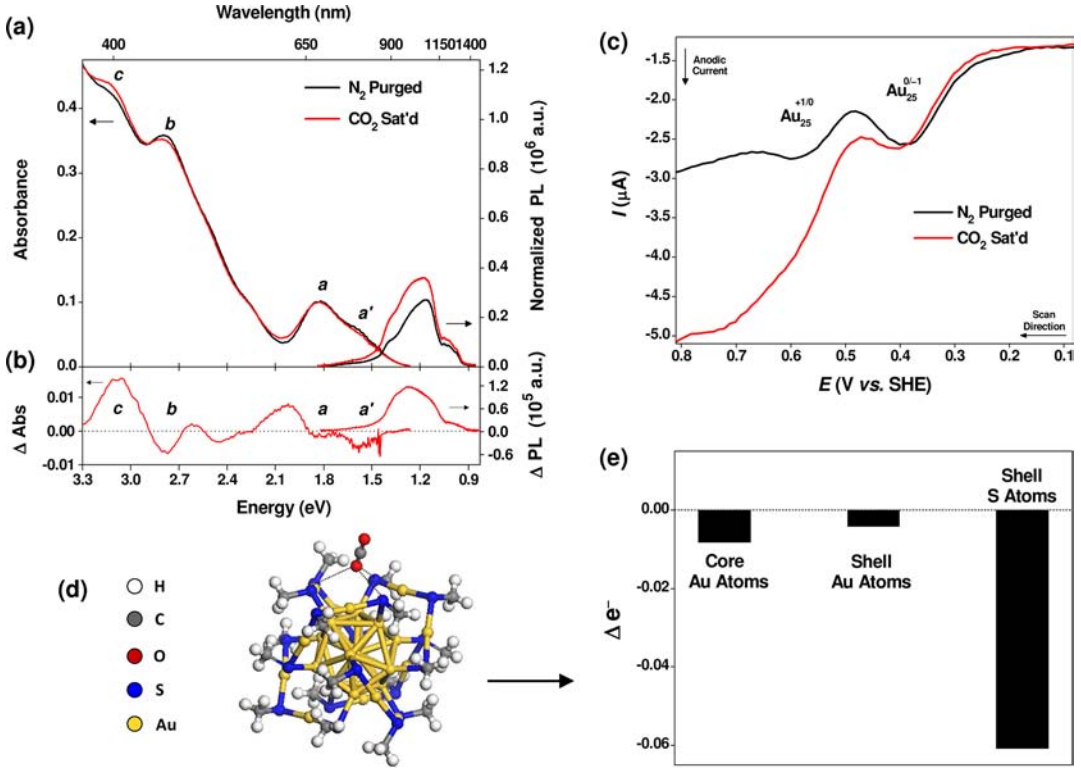

Figure 2. Experimental results and density functional theory (DFT) modeling of the Au_{25}–CO_2 couple. (a) Optical absorbance and PL spectra, and (b) difference spectra (Δabs and ΔPL) of Au_{25} in N_2 purged and CO_2 saturated DMF; PL spectra were normalized to the absorbance peak area at λ_{ex} = 2.78 eV (i.e., absorbance feature *b*). (c) Square wave voltammetry of Au_{25} in N_2 purged and CO_2 saturated DMF + 0.1 M TBAP; anodic (oxidizing) currents are negative, and scans were collected at 0.05 V s^{-1}. (d) DFT model of stable CO_2 adsorption where an O atom of CO_2 interacts with three S atoms in the Au_{25} shell. (e) Bader charge analysis showing the change in Au_{25} valence electrons upon CO_2 adsorption; negative values indicate electron loss. Additional DFT results are presented in Figures S14–S17.

(Figure 1c). The apparent interaction between Au_{25} and CO_2 was somewhat unexpected because CO_2 shows little electronic interaction with traditional gold surfaces.[37] Control experiments have shown that the optical changes did not result from drift in the spectrometer signal, the purge gas, solvent evaporation, solvent polarity, instability of Au_{25} optical properties, or the inadvertent introduction of trace atmospheric moisture (Figures S7–S12). Furthermore, pH-induced spectral changes are unlikely in aprotic solvents,[38] and we confidently attribute the phenomenon to an interaction between Au_{25} and CO_2. We note that the CO_2-induced spectral changes were somewhat smaller than those in previous reports of Au_{25} oxidation.[29−33,39] Nonetheless, the above cited examples of Au_{25} oxidation were not easily reversed, and the restoration of Au_{25} optical properties, when attempted, required strong reducing agents or electrochemical potentials. In the current study, the CO_2-induced optical changes were reversed by simply purging the solution with N_2 (Figure S13), suggesting a comparatively weak interaction between the Au_{25} cluster and CO_2.

CO_2 also affected the electrochemical properties of Au_{25}. The redox waves presented in Figure 2c represent quantified charge injection into the Au_{25} HOMO.[27,36] We found that the introduction of CO_2 induced a small but significant 21 ± 2 mV shift in the $Au_{25}^{0/-1}$ redox wave (>99% confidence level, CL; n = 3). Positive potentials are considered oxidizing,[40] and a positive shift in the $Au_{25}^{0/-1}$ redox potential is consistent with electronic depletion of the Au_{25} HOMO (e.g., a larger potential will be required to withdraw electrons from an oxidized species).[34] The electrochemical and spectroscopic results are consistent with the energy level diagram presented in Figure 1b, since depletion of the HOMO is expected to induce concomitant spectral bleaching and positive redox shifts. We could not identify CO_2-induced shifts in the $Au_{25}^{+1/0}$ redox wave because this feature was masked by a broad current increase. We hypothesize this phenomenon was related to potential-induced desorption of CO_2 from the Au_{25} surface. Lastly, the electrochemical changes were reversed by purging the solution with N_2 (Figure S13). In comparison to previous studies, both Murray and co-workers[34,35] and Devadas et al.[41] have reported that electron-withdrawing ligand groups can irreversibly shift the $Au_{25}^{0/-1}$ wave by several hundred millivolts. The observed CO_2-induced changes are smaller than those for the above cited examples, but again, the smaller and more reversible shift in redox potential indicates a comparatively weak interaction between Au_{25} and CO_2.

Impressive strides have been made in the theoretical modeling of Au clusters.[6,8,20,21,28,35,42,43] However, investigation of strongly bound adsorbates like O_2 and CO required activating the cluster by removing ligand groups.[20,21] Some molecules, such as CO_2, are not expected to chemisorb to the Au_{25} surface, and the effects of weaker physisorption-type interactions have remained unaddressed. In our work, an extensive search for stable CO_2 adsorption configurations was undertaken using DFT. Specifically, our model utilized Au_{25} clusters capped with 18 S–CH_3 ligands to mimic the fully ligand-protected cluster used in our experiments. CO_2 adsorption was found to occur at a specific "pocket", or site,

dx.doi.org/10.1021/ja303259q | J. Am. Chem. Soc. 2012, 134, 10237−10243

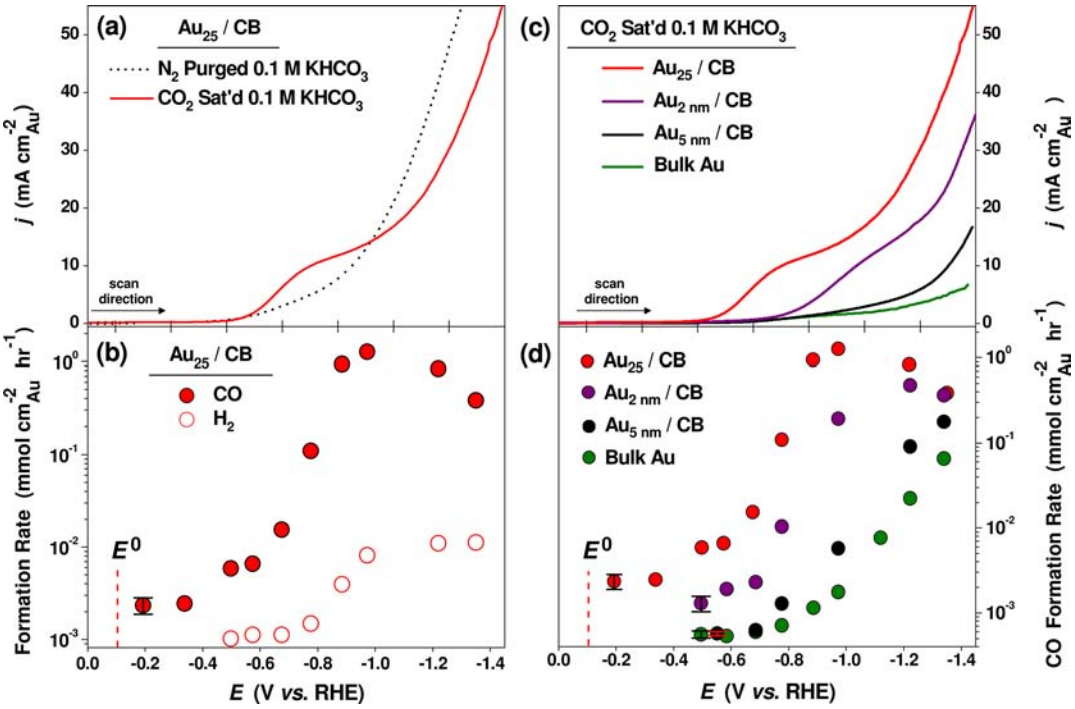

Figure 3. Electrochemical reduction of CO_2 in aqueous 0.1 M $KHCO_3$; cathodic (reducing) currents are positive, all scans were collected at a rate of 0.01 V s^{-1}, and error bars are from three separate runs with freshly prepared samples. (a) Linear sweep voltammograms (LSVs) of carbon black (CB) supported Au_{25} in quiescent (unstirred) N_2 purged (pH = 9) and CO_2 saturated (pH = 7) 0.1 M $KHCO_3$. (b) Potential-dependent H_2 and CO formation rates for Au_{25}/CB; solutions were stirred at a constant rate during electrolysis runs to prevent product (bubble) buildup on the electrode surface. (c) LSVs of various Au catalysts in quiescent CO_2 saturated 0.1 M $KHCO_3$ (pH = 7). (d) Potential-dependent CO formation rates for the various Au catalysts; solutions were stirred at a constant rate during electrolysis runs to prevent product (bubble) buildup on the electrode surface. Product values are listed in Tables S2 and S3 in the Supporting Information section.

on the Au_{25} surface with binding energies that ranged between −0.07 and −0.14 eV (Figure S14). Our calculations predict similar CO_2 binding at finite temperatures, and comparable binding energies were also found at 300 K. Figure 2d presents one stable configuration where an oxygen atom of CO_2 interacts with three sulfur atoms in the Au_{25} shell. This specific adsorption configuration had a calculated binding energy of 0.13 eV and a O−S separation between 3.31 and 3.45 Å. We found the bound CO_2 to be essentially linear, and the calculated O−C−O angle differs by only 1−2° with respect to the free CO_2. The small perturbation in the internal structure of the molecule is consistent with CO_2 physisorption.

Analysis of the electronic properties indicated that CO_2 adsorption only induced minor perturbations to the Au_{25} density of states (Figure S15) and withdrew less than 0.1 electrons from the Au_{25} cluster. However, complementary Bader charge analysis[44,45] revealed the major consequence of CO_2 adsorption was charge redistribution *within* the Au_{25} cluster. Figure 2e presents the change in Au_{25} valence electrons after the adsorption of a CO_2 molecule, clearly showing the depletion of S atom electrons. The three predicted CO_2 adsorption configurations consistently depleted electron density from the S atoms, although charge redistribution between the core and shell Au atoms varied between the different Au_{25}−CO_2 configurations (Figure S16).

Direct comparison to literature values is not straightforward because previous DFT efforts utilized models that were based on bare or partially ligand-protected clusters. For example, intermediately bound states with energies of approximately −1.0 eV were found for CO adsorption on bare Au_n (n = 16−35) clusters.[20] A similar bound state was also predicted for O_2 adsorption on partially ligand-protected Au_{25} clusters, and O_2 binding energies of −0.62 and −0.72 eV were found after Au_{25} was activated by removing one or two ligand groups.[21] In the present case, the Au_{25} cluster was not artificially activated by ligand removal. Under these conditions, our work provides theoretical evidence of weakly bound CO_2, and this result is in line with the observation of reversible CO_2-induced spectroscopic and electrochemical changes. Finally, the computational results indicate the major consequence of CO_2 adsorption was the redistribution of charge within the Au_{25} cluster. This finding is interesting because Murray and co-workers have suggested that polar ligand groups can induce oxidation-like effects through charge redistribution and Au−S bond polarization.[33−35] This hypothesis is reasonable because most Au_{25} orbitals contain a significant S atom contribution (Figure S17),[8] meaning charge redistribution and/or Au−S bond polarization could disrupt geometric and electronic coupling within the cluster and produce the experimentally observed optical and electrochemical changes noted above.[4,24]

CO_2 is not a polar molecule, but it does have a rather strong quadrupole moment and it can couple with anionic species.[46] We suspect that CO_2 adsorption was promoted, in part, by an electrostatic attraction to the negatively charged Au_{25} cluster. The electrostatic potential that developed between the adsorbed CO_2 quadrupole and Au_{25} redistributed charge within the cluster to produce reversible oxidation-*like* optical and electrochemical phenomena. Finally, the Au_{25} electronic structure was restored by simply purging the solution with N_2 to desorb the weakly bound CO_2.

Electrochemical Reduction of CO_2. The unique interaction between Au_{25} and CO_2 provided an exciting opportunity

dx.doi.org/10.1021/ja303259q | J. Am. Chem. Soc. 2012, 134, 10237−10243

to test CO_2 reduction with a negatively charged nanocatalyst. From a practical standpoint, the electrochemical reduction of aqueous CO_2 is attractive because the mechanisms are well understood and water represents an inexpensive and environmentally benign solvent for scaled-up processes.[18,19] Figure 3 compares the electrocatalytic activity of Au_{25} (~1 nm)[7,8] and larger Au catalysts for the electrochemical reduction of CO_2 in aqueous 0.1 M $KHCO_3$. Potential-dependent product analysis (Figure 3b) identified significant and reproducible CO formation at an onset potential of −0.193 V vs RHE (>95% CL, n = 3). Electrolysis in N_2 purged $KHCO_3$ ruled out spurious CO evolution from Au_{25}'s organic ligands or the carbon black support. Remarkably, the onset of CO formation was within 90 mV of the $CO_2 \rightarrow CO$ formal potential (−0.103 V vs RHE).[19] This low overpotential constitutes an approximate 200−300 mV reduction compared to the case of the larger Au catalysts in this study (Figure 3d) and those in previous literature reports.[18,19,22]

Peak CO production from the Au_{25} catalyst was found at −1.0 V vs RHE with approximately 100% Faradaic efficiency (FE) and a rate 7−700 times higher than 2−5 nm Au nanoparticles and bulk Au (Figure 3d and Table S2). Our previous experiments with CB-supported catalysts showed CO production from the CB support was negligible compared to the case of Au_{25} (at −0.9 V CB: 5×10^{-9} mol CO h^{-1} vs Au_{25}: 6.2×10^{-6} mol CO h^{-1});[47] please note these rates are *not* normalized to the electrochemical surface area of Au. FE relates the amount of reaction product to the total number of electrons passed through the electrode (Figure S18). For Au_{25}, CO formation at −1.0 V occurred with approximately 100% FE, meaning almost every electron injected into the catalyst layer was utilized for CO_2 reduction. Au is known to selectivity reduce CO_2 into CO,[18,19] and CO selectivities ranged between 80.8 and 99.6% for Au_{25}, 71.0−96.9% for the larger Au nanoparticles and 26.9−92.9% for bulk Au, depending on the applied voltage (Table S3). However, the higher FE of the Au_{25} cluster enhanced its CO production rate compared to the those for the other Au catalysts (Figure 3d and Table S2).

Potential-dependent CO_2 reduction rates have also been noted by Chen and Kanan for Sn-oxide catalysts,[48] but the decreased rates beyond −1.0 V likely stem from gaseous products blocking the Au_{25} surface (Figure 3b,d). On the basis of the peak CO production rate of 1.26 mmol cm^{-2} h^{-1}, we can estimate a maximum turnover frequency (TOF) of 87 CO molecules $site^{-1}$ s^{-1} for the Au_{25} catalyst; sites are defined as accessible Au atoms and determined from electrochemical surface area measurements.[49] This TOF value is approximately 10−100 times higher than those of current state-of-the-art electrochemical processes[23] and is comparable to previous reports of CO oxidation on ligand-free Au_n clusters (n = 4−19).[50]

The retention of characteristic optical spectra after CO_2 reduction at −1.0 V ruled out Au_{25} decomposition under electrocatalytic conditions (Figure S19 of the Supporting Information).[14,51−53] Specifically, the optical spectra contain contributions from states derived from both core and shell atoms,[4,24,25] and structural deterioration, i.e. ligand desorption or destruction of the −S−Au−S−Au−S− bonding motif in the cluster's shell, should severely alter the absorbance and/or PL spectra.[14,51−53] In contrast to Au_{25}'s ligands, alkanethiol monolayers can desorb from traditional Au surfaces during the application of even modest electrochemical potentials (*c.a.* −0.4 V vs RHE).[54] However, Au_{25} is not a traditional Au surface, and the stability of its −SR ligands has been noted before.[51,52] Au_{25}'s stability stems from the unique −S−Au−S−Au−S− bonding motif in the cluster shell (Figure 1a). This shell stabilizes the organic ligands and protects the cluster from deterioration during chemical oxidation or reduction,[51,52] catalytic reactions,[9−14] and the application of electrochemical potentials (Figure S19).[15]

CO and H_2 were the only reaction products detected, and the potential-dependent product distribution in Figure 3b provides insight into the electrocatalytic mechanism. CO is the major CO_2 reduction product for Au electrodes, and the reaction proceeds along a two-electron, two-proton pathway through an adsorbed $^{\bullet}CO_2^-$ intermediate;[18,19] please see equations S1−S6 in the Supporting Information for further details. In the low potential regime (below −0.5 V), sequential proton capture and electron transfer converts adsorbed $^{\bullet}CO_2^-$ into $^{\bullet}COOH_{(ads)}$ before forming CO and water. A sharp increase in CO production occurred with the onset of H_2 evolution at approximately −0.5 V. In this potential range, the formation of H_{ads} occurs simultaneously with H_2 evolution, and a $CO_2 \rightarrow CO$ pathway based on the direct reduction of $^{\bullet}CO_2^-$ with H_{ads} is likely. CO evolution onset potentials for the larger Au catalysts were comparable to previous results,[18,19,22] and their equivalent values suggest the presence of similar active sites. Alternatively, the smaller CO evolution potential of Au_{25} points to a unique catalytic site capable of promoting the $CO_2 \rightarrow CO$ reaction closer to the thermodynamic limit. Jin and co-workers have suggested that Au_{25} contains a reactive site capable of promoting both C═O bond activation and H_{ads} formation.[13,14] Our computationally identified CO_2 adsorption site is consistent with the site proposed by Jin and co-workers (Figure S20 of the Supporting Information). Accordingly, we hypothesize that enhanced electrocatalytic activity stems from Au_{25}'s anionic charge promoting CO_2 adsorption and its unique reactive site facilitating C═O bond activation and H_{ads} formation.

■ CONCLUSIONS

We have shown spectroscopic, electrochemical, and computational evidence to support a reversible electronic interaction between CO_2 and atomically precise Au_{25} clusters. Specifically, CO_2 adsorption redistributed charge *within* the Au_{25} cluster to produce optical and electrochemical changes similar to those observed during cluster oxidation. The successful correlation of experimental and computational data is exciting because it provides insight into the electronic interactions between Au_{25} clusters and weakly bound adsorbates. Lastly, we have shown that the Au_{25} clusters can perform as superior catalysts for the electrochemical conversion of CO_2 into CO. Specifically, Au_{25} promoted the $CO_2 \rightarrow CO$ reaction within 90 mV of the formal potential (thermodynamic limit) and showed peak CO production at −1.0 V vs RHE that was 7−700 times higher than that for larger Au catalysts and 10−100 times higher than those for current state-of-the-art processes.

■ EXPERIMENTAL SECTION

Au_{25} was synthesized as previously reported,[55] and all organic solvents were dried over 3 Å molecular sieves. Absorption spectroscopy was performed with Perkin-Elmer Lambda 1050 and Agilent 8453 spectrometers. PL spectroscopy was performed with a Jobin Yvon Horiba Fluorolog 332 spectrometer equipped with a liquid N_2 cooled InGaAs detector. All presented PL spectra are the average of 10 scans with an excitation energy of 2.78 eV (447 nm) unless otherwise noted,

dx.doi.org/10.1021/ja303259q | J. Am. Chem. Soc. 2012, 134, 10237−10243

and a 2.26 eV (550 nm) long-pass optical filter was placed between the sample and the detector to prevent the appearance of higher order excitation peaks in the PL spectrum. Au_{25} solutions in DMF were placed in sealable cuvettes and initially purged overnight with N_2, bubbled with ultrahigh purity CO_2 for 1.5 h, and finally purged with N_2 again for 1.5 h; experiments with *p*-xylene as a solvent used an initial 1.5 h N_2 purge to reduce solvent evaporation. During gas exposure experiments, the PL spectra were normalized to the absorbance peak area at λ_{ex} = 2.78 eV (i.e., absorbance feature *b*); please see Figure S6 in the Supporting Information for further details.

Electrochemical measurements were performed with a Biologic SP-150 potentiostat equipped with a low-current option. Nonaqueous electrochemistry was conducted in DMF + 0.1 M tetrabutylammonium perchlorate (TBAP) with Pt wire working and counter electrodes and a nonaqueous Ag/Ag^+ reference electrode (0.01 M $AgNO_3$ + 0.1 M TBAP in CH_3CN); potentials were calibrated into the standard hydrogen electrode (SHE) scale using ferrocene (Fc/Fc^+ = 0.7112 V vs SHE in DMF + 0.1 M TBAP).[56] *In situ* spectroelectrochemical measurements were conducted with a commercially available quartz cell from BASi.

Aqueous electrochemical experiments were conducted in 0.1 M $KHCO_3$ solutions prepared with ultrapure water (≥18.0 MΩ·cm). Catalyst inks were prepared by sonicating acetone-solvated Au_{25} into a mixture of methanol, Vulcan XC-72R carbon black, and Nafion; catalyst inks were also prepared in an identical manner using commercially available 2 and 5 nm Au nanoparticles from BBInternational. The catalyst ink was deposited onto a glassy carbon (GC) working electrode and allowed to dry in air. Electrochemical experiments with bulk Au were conducted with a 99.99% Au wire that was cleaned in 1.0 M H_2SO_4, rinsed with ultrapure water, and used as a working electrode. A Pt wire counter electrode and a conventional Ag/AgCl reference electrode (3.0 M NaCl) were used to complete the aqueous electrochemical setup. The Ag/AgCl reference electrode was regularly calibrated against a commercially available Hydroflex reversible hydrogen electrode; E° = 0.000 V − 0.059pH (ref 40). The solution pH was measured after each experiment to convert the Ag/AgCl reference electrode potentials into the RHE scale; typical pH values for N_2 and CO_2 saturated 0.1 M $KHCO_3$ were 7.0 and 9.0. The linear sweep voltammograms presented in Figure 3a and c were conducted in quiescent (unstirred) solutions.

Electrochemical CO_2 reduction reactions were performed in a gastight, two-compartment H-cell. The working and counter electrodes were housed in different compartments that were separated by a 0.1778 mm (0.007 in.) thick Nafion 117 cation exchange membrane; this experimental configuration prevented CO_2 reduction products from being oxidized at the counter electrode. During CO_2 electrolysis runs, a particular voltage was applied for 1 h and the solution was stirred at a constant rate to prevent product (bubble) buildup on the electrode surface. After 1 h of electrolysis, products were analyzed with a Perkin-Elmer Clarus 600 gas chromatograph equipped with TCD and FID detectors. Multiple blank injections accompanied each electrolysis run to establish an instrumental baseline for the CO peak area, and we have defined the CO formation onset potential as the potential where CO formation was significant above the baseline at a 95% confidence level. Electrochemical currents and product formation rates were normalized to the catalyst electrochemical surface area (ECSA), as measured by integrating the so-called Au oxide stripping peak in N_2 purged 0.1 M $KHCO_3$ (ref 49); this approach has previously been used to measure the ECSA of Au_n cluster electrocatalysts (n = 11−140) in aqueous media.[15] We found the Au_{25} clusters retained characteristic optical absorbance and PL spectral features after oxide formation/stripping (Figure S19 of the Supporting Information).

Computational Methodolgy. The adsorption of CO_2 on the model $Au_{25}(SCH_3)_{18}^{-1}$ cluster was examined using the Vienna ab initio simulation package (VASP) which employs density functional theory with a basis set constructed from plane waves.[57,58] The Perdew−Burke−Enzerhoff (PBE) generalized gradient approximation (GGA) functional was employed to calculate the exchange-correlation energy.[59] The electron−ion interaction was described by the projector-augmented wave (PAW) method.[60]

The model for the $Au_{25}(SCH_3)_{18}^{-1}$ cluster was constructed using the DFT relaxed $Au_{25}(SH)_{18}^{-1}$ structure determined by Aikens as a starting point.[42] The terminating H atoms were then replaced by CH_3 to give rise to a $Au_{25}(SCH_3)_{18}^{-1}$ structure. The cluster was placed in a cubic box with dimensions of 24 Å sides, and a uniform compensating background charge was assumed. Various binding configurations of CO_2 adsorbate on the cluster were explored, and Γ-point calculations were carried out with an energy cutoff of 600 eV. Geometries were relaxed using a quasi-Newton variable metric algorithm until the atomic forces were less than 0.03 eV/Å. The CO_2 binding energy was calculated using the expression $E_{bind} = E_{CO_2+cluster} - (E_{cluster} + E_{CO_2})$. Here $E_{CO_2+cluster}$ is the total energy of the relaxed CO_2−Au_{25} cluster system, while $E_{cluster}$ and E_{CO_2} are the total energies of the relaxed bare cluster and the gas phase CO_2, respectively. On the basis of this convention, a negative E_{bind} corresponds to an exothermic reaction (stable adsorption configuration).

■ ASSOCIATED CONTENT

Supporting Information

Additional experimental and computational data. This material is available free of charge via the Internet at http://pubs.acs.org.

■ AUTHOR INFORMATION

Corresponding Author

Douglas.Kauffman@CONTR.NETL.DOE.GOV

Notes

The authors declare no competing financial interest.

■ ACKNOWLEDGMENTS

The authors thank Professor J. P. Lewis for fruitful discussions. This technical effort was performed in support of the NETL's ongoing research in CO_2 utilization under RES Contract DE-FE0004000. R.J. acknowledges financial support from the Air Force Office of Scientific Research under AFOSR Award No. FA9550-11-1-9999 (FA9550-11-1-0147). Reference in this work to any specific commercial product is to facilitate understanding and does not necessarily imply endorsement by the United States Department of Energy. This report was prepared as an account of work sponsored by an agency of the United States Government. Neither the United States Government nor any agency thereof, nor any of their employees, makes any warranty, express or implied, or assumes any legal liability or responsibility for the accuracy, completeness, or usefulness of any information, apparatus, product, or process disclosed, or represents that its use would not infringe privately owned rights. Reference herein to any specific commercial product, process, or service by trade name, trademark, manufacturer, or otherwise does not necessarily constitute or imply its endorsement, recommendation, or favoring by the United States Government or any agency thereof. The views and opinions of authors expressed herein do not necessarily state or reflect those of the United States Government or any agency thereof.

■ REFERENCES

(1) Daniel, M.-C.; Astruc, D. *Chem. Rev.* **2004**, *104*, 293.

(2) Sardar, R.; Funston, A. M.; Mulvaney, P.; Murray, R. W. *Langmuir* **2009**, *25*, 13840.

(3) Rodriguez, P.; Kwon, Y.; Koper, M. T. M. *Nature Chem.* **2012**, *4*, 177.

(4) Jin, R. *Nanoscale* **2010**, *2*, 343.

(5) Parker, J. F.; Fields-Zinna, C. A.; Murray, R. W. *Acc. Chem. Res.* **2010**, *43*, 1289.
(6) Jupally, V. R.; Kota, R.; Dornshuld, E. V.; Mattern, D. L.; Tschumper, G. S.; Jiang, D.-e.; Dass, A. *J. Am. Chem. Soc.* **2011**, *133*, 20258.
(7) Heaven, M. W.; Dass, A.; White, P. S.; Holt, K. M.; Murray, R. W. *J. Am. Chem. Soc.* **2008**, *130*, 3754.
(8) Zhu, M.; Aikens, C. M.; Hollander, F. J.; Schatz, G. C.; Jin, R. *J. Am. Chem. Soc.* **2008**, *130*, 5883.
(9) Zhu, Y.; Qian, H.; Jin, R. *J. Mater. Chem.* **2011**, *21*, 6793.
(10) Liu, Y.; Tsunoyama, H.; Akita, T.; Tsukuda, T. *Chem. Commun.* **2010**, *46*, 550.
(11) Turner, M.; Golovko, V. B.; Vaughan, O. P. H.; Abdulkin, P.; Berenuer-Murcia, A.; Tikhov, M. S.; Johnson, B. F. G.; Lambert, R. M. *Nature* **2008**, *454*, 981.
(12) Liu, Y.; Tsunoyama, H.; Akita, T.; Xie, S.; Tsukuda, T. *ACS Catal.* **2011**, *1*, 2.
(13) Zhu, Y.; Qian, H.; Drake, B. A.; Jin, R. *Angew. Chem., Int. Ed.* **2010**, *49*, 1295.
(14) Zhu, Y.; Wu, Z.; Gayathri, C.; Qian, H.; Gil, R. R.; Jin, R. *J. Catal.* **2010**, *271*, 155.
(15) Chen, W.; Chen, S. *Angew. Chem., Int. Ed.* **2009**, *48*, 4386.
(16) Arakawa, H.; Aresta, M.; Armor, J. N.; Barteau, M. A.; Beckman, E. J.; Bell, A. T.; Bercaw, J. E.; Creutz, C.; Dinjus, E.; Dixon, D. A.; Domen, K.; DuBois, D. L.; Eckert, J.; Fujita, E.; Gibson, D. H.; Goddard, W. A.; Goodman, D. W.; Keller, J.; Kubas, G. J.; Kung, H. H.; Lyons, J. E.; Manzer, L. E.; Marks, T. J.; Morokuma, K.; Nicholas, K. M.; Periana, R.; Que, L.; Rostrup-Nielson, J.; Sachtler, W. M. H.; Schmidt, L. D.; Sen, A.; Somorjai, G. A.; Stair, P. C.; Stults, B. R.; Tumas, W. *Chem. Rev.* **2001**, *101*, 953.
(17) Peterson, A. A.; Nørskov, J. K. *J. Phys. Chem. Lett.* **2012**, *3*, 251.
(18) Hori, Y. *Electrochemical CO_2 reduction on metal electrodes*; Springer: New York, 2008; Vol. *42*.
(19) Gattrell, M.; Gupta, N.; Co, A. *J. Electroanal. Chem.* **2006**, *594*, 1.
(20) Gao, Y.; Shao, N.; Pei, Y.; Chen, Z.; Zeng, X. C. *ACS Nano* **2011**, *5*, 7818.
(21) Lopez-Acevedo, O.; Kacprzak, K. A.; Akola, J.; Häkkinen, H. *Nature Chem.* **2010**, *2*, 329.
(22) Hori, Y.; Murata, A.; Katsuhei, K.; Suzuki, S. *J. Chem. Soc., Chem. Commun.* **1987**, 728.
(23) Rosen, B. A.; Salehi-Khojin, A.; Thorson, M. R.; Zhu, W.; Whipple, D. T.; Kenis, P. J. A.; Masel, R. I. *Science* **2011**, *334*, 643.
(24) Devadas, M. S.; Bairu, S.; Qian, H.; Sinn, E.; Jin, R.; Ramakrishna, G. *J. Phys. Chem. Lett.* **2011**, *2*, 2752.
(25) Qian, H.; Sfeir, M. Y.; Jin, R. *J. Phys. Chem. C* **2010**, *114*, 19935.
(26) Please note that some early reports misidentified anionic Au_{25} as neutral Au_{38}.
(27) Lee, D.; Donkers, R. L.; Wang, G.; Harper, A. S.; Murray, R. W. *J. Am. Chem. Soc.* **2004**, *126*, 6193.
(28) Aikens, C. M. *J. Phys. Chem. Lett.* **2010**, *1*, 2594.
(29) Zhu, M.; Eckenhoff, W. T.; Pintauer, T.; Jin, R. *J. Phys. Chem. C* **2008**, *112*, 14221.
(30) Wu, Z.; Jin, R. *Nano Lett.* **2010**, *10*, 2568.
(31) Choi, J.-P.; Fields-Zinna, C. A.; Stiles, R. L.; Balasubramanian, R.; Dougals, A. D.; Crowe, M. C.; Murray, R. W. *J. Phys. Chem. C* **2010**, *114*, 15890.
(32) Liu, Z.; Zhu, M.; Meng, X.; Xu, G.; Jin, R. *J. Phys. Chem. Lett.* **2011**, *2*, 2104.
(33) Wang, G.; Guo, R.; Kalyuzhny, G.; Choi, J.-P.; Murray, R. W. *J. Phys. Chem. B* **2006**, *110*, 20282.
(34) Guo, R.; Murray, R. W. *J. Am. Chem. Soc.* **2005**, *127*, 12140.
(35) Parker, J. F.; Kacprzak, K. A.; Lopez-Acevedo, O.; Häkkinen, H.; Murray, R. W. *J. Phys. Chem. C* **2010**, *114*, 8276.
(36) García-Raya, D.; Madueño, R.; Blázquez, M.; Pineda, T. *J. Phys. Chem. C* **2009**, *113*, 8756.
(37) Freund, H.-J.; Roberts, M. W. *Surf. Sci. Rep.* **1996**, *25*, 225.
(38) Gennaro, A.; Isse, A. A.; Vianello, E. *J. Electroanal. Chem.* **1990**, *289*, 203.
(39) Venzo, A.; Antonello, S.; Gascón, J. A.; Guryanov, I.; Leapman, R. D.; Perera, N. V.; Sousa, A.; Zamuner, M.; Zanella, A.; Maran, F. *Anal. Chem.* **2011**, *83*, 6355.
(40) Bard, A. J.; Faulkner, L. R. *Electrochemical methods: fundamentals and applications*, 2nd ed.; John Wiley & Sons: New York, 2001.
(41) Devadas, M. S.; Kwak, K.; Park, J.-W.; Choi, J.-H.; Jun, C.-H.; Sinn, E.; Ramakrishna, G.; Lee, D. *J. Phys. Chem. Lett.* **2010**, *1*, 1497.
(42) Aikens, C. M. *J. Phys. Chem. C* **2008**, *112*, 19797.
(43) Pei, Y.; Pal, R.; Liu, C.; Gao, Y.; Zhang, Z.; Zeng, X. C. *J. Am. Chem. Soc.* **2012**, *134*, 3015.
(44) Henkelman, G.; Arnaldsson, A.; Jónsson, H. *Comput. Mater. Sci.* **2006**, *36*, 354.
(45) Sanville, E.; Kenny, S. D.; Smith, R.; Henkelman, G. *J. Comput. Chem.* **2007**, *28*, 899.
(46) Arnold, D. W.; Bradforth, S. E.; Kim, E. H.; Neumark, D. M. *J. Chem. Phys.* **2008**, *102*, 3510.
(47) Kauffman, D. R.; Ohodnicki, P. R.; Kail, B. W.; Matranga, C. *J. Phys. Chem. Lett* **2011**, *2*, 2038.
(48) Chen, Y.; Kanan, M. W. *J. Am. Chem. Soc.* **2012**, *134*, 1986.
(49) Trasatti, S.; Petrii, O. A. *Pure Appl. Chem.* **1991**, *63*, 711.
(50) Wallace, W. T.; Wetten, R. L. *J. Am. Chem. Soc.* **2002**, *124*, 7499.
(51) Negishi, Y.; Chaki, N. K.; Shichibu, Y.; Whetten, R. L.; Tsukuda, T. *J. Am. Chem. Soc.* **2007**, *129*, 11322.
(52) Wu, Z.; Jin, R. *ACS Nano* **2009**, *3*, 2036.
(53) Shichibu, Y.; Negishi, Y.; Tsunoyama, H.; Kanehara, M. *Small* **2007**, *3*, 835.
(54) Love, J. C.; Estroff, L. A.; Kriebel, J. K.; Nuzzo, R. G.; Whitesides, G. M. *Chem. Rev.* **2005**, *105*, 1103.
(55) Zhu, M.; Lanni, E.; Garg, N.; Bier, M. E.; Jin, R. *J. Am. Chem. Soc.* **2008**, *130*, 1138.
(56) Connelly, N. G.; Geiger, W. E. *Chem. Rev.* **1996**, *96*, 877.
(57) Kresse, G.; Furthmüller, J. *Phys. Rev. B* **1996**, *54*, 11169.
(58) Hafner, J. *J. Comput. Chem.* **2008**, *29*, 2044.
(59) Perdew, J. P.; Burke, K.; Wang, Y. *Phys. Rev. B* **1996**, *54*, 16533.
(60) Kresse, G.; Joubert, D. *Phys. Rev. B* **1999**, *59*, 1758.